Carbohydrate Polymers 87 (2012) 2512–2518

Contents lists available at SciVerse ScienceDirect

Carbohydrate Polymers

journal homepage: www.elsevier.com/locate/carbpol

Structure and properties of hydroxyapatite/cellulose nanocomposite films

Meng He, Chunyu Chang, Na Peng, Lina Zhang*

Department of Chemistry, Wuhan University, Wuhan 430072, China

ARTICLE INFO

Article history:
Received 10 June 2011
Received in revised form 27 July 2011
Accepted 8 November 2011
Available online 17 November 2011

Keywords:
Nano-hydroxyapatite
Cellulose film
Inorganic–organic hybrid
Biomaterials

ABSTRACT

The aim of this study was to develop a new inorganic–organic hybrid film. Nanohydroxyapaptite (nHAP) particles as the inorganic phase was mixed with cellulose in 7 wt.% NaOH/12 wt.% urea aqueous solution with cooling to prepare a blend solution, and then inorganic–organic hybrid films were fabricated by coagulating with Na_2SO_4 aqueous solution. The structure and properties of the hybrid films were characterized by high resolution transmitting electron microscopy (HRTEM), field emission scanning electron microscopy (FESEM), thermo-gravimetric analysis (TGA), Fourier transform infra-red (FT-IR) spectra, wide angle X-ray diffraction (WAXD) and tensile testing. The results revealed that the HAP nanoparticles with mean diameter of about 30 nm were uniformly dispersed and well immobilized in the hybrid film as a result of the role of the nano-and micropores in the cellulose substrate. A strong interaction existed between HAP and cellulose matrix, and their thermal stability and mechanical strength were improved as a result of good miscibility. Furthermore, the results of 293T cell viability assay indicated that the HAP/cellulose films had excellent biocompatibility and safety, showing potential applications in biomaterials.

1. Introduction

Recently, the composite materials made of organic and inorganic phases have attracted much attention. It is noted that, polymer–composite materials have been widely used in biomedical field (Ramakrishna, Mayer, Wintermantel, & Leong, 2001), and natural polymers, such as cellulose, chitin, corn protein, starch and soy protein isolate (SPI) (Bhardwaj, Mohanty, Drzal, Pourboghrat, & Misra, 2006; Lu & Larock, 2007; Yan, Chen, & Bangal, 2007) have become important due to the increasing requirements for materials with characteristics of renewability, biocompatibility, biodegradability, and non-toxicity (Cheung, Lau, Lu, & Hui, 2007; Juntaro et al., 2008; Ragauskas et al., 2006; Sgriccia, Hawley, & Misra, 2008; Svagan, Samir, & Berglund, 2008; Yang et al., 2009). Cellulose is the most abundant natural polymer and a good candidate for the organic/inorganic hybrid material (Habibi, Lucia, & Rojas, 2010), however, until recently a factor limiting its potential applications was the lack of an eco friendly ways for producing shaped materials from cellulose. In our laboratory, new solvent systems for cellulose dissolution, such as NaOH/urea, NaOH/thiourea, and LiOH/urea aqueous solutions with cooling have been developed (Cai & Zhang, 2005, 2006; Cai et al., 2008). The various functional materials prepared by using cellulose as a matrix, regenerated from these solvents have been studied previously in our laboratory (Chang, Peng, Zhang, & Pang, 2009; Liu, Zhang, Zhou, & Wu, 2008; Luo, Liu, Zhou, & Zhang, 2009; Qi, Chang, & Zhang, 2008; Ruan, Zhang, Mao, Zeng, & Li, 2004).

As the principal inorganic constituent of nature, bone, hydroxyapaptite is mainly used in the tissue engineering field due to its excellent biocompatible, bioactive, non-inflammatory, non-toxic and osteoconductive properties (Murugan & Ramakrishna, 2004). HAP has been used as a resin for the purification of proteins and plasmid DNA, because the surface has both positive and negative ions (such as Ca^{2+}, PO_4^{3-}), which can electrostatically bind with basic and acidic biomacromolecules, respectively (Colman, Byers, Primrose, & Lyons, 1978; Schröder, Jönsson, & Poole, 2003). Recently, the high affinity of HAP for protein has been used in binding and releasing biologically active molecules (Jongpaiboonkit, Franklin-Ford, & Murphy, 2009). It is noted that the incorporation of HAP into poly(L-lactide) can improve protein adsorption capacity greatly because HAP has not only a high affinity for protein but also changes the scaffold surface morphology making them more suitable for protein absorption (Wei & Ma, 2004). The biocompatibility and biodegradability of natural polymers are essential for tissue engineering, therefore the inclusion of nHAP into the biopolymer matrix can improve the mechanical properties, and incorporate the nanotopographic features that mimic the nanostructure of bone (Swetha et al., 2010). Furthermore, cells are naturally accustomed to interacting with nano-structured surface roughness in the body, and polymers can duplicate such a roughness through the incorporation of nanophase materials (Balasundaram & Webster, 2007).

* Corresponding author. Tel.: +86 27 87219274; fax: +86 27 68762005.
E-mail addresses: lnzhang@public.wh.hb.cn, linazhangwhu@gmail.com (L. Zhang).

0144-8617/$ – see front matter.
doi:10.1016/j.carbpol.2011.11.029

Chitosan/montmorillonite/HAP, nHAP/chitosan gelatin (CG) scaffolds, PLA/HAP scaffold, chitosan hydrogel/HAP films, β-chitin/HAP films, bacterial cellulose/HAP gel have been studied for their biomedical applications (Grande, Torres, Gomez, & Carmen Bano, 2009; Jeong et al., 2008; Katti, Katti, & Dash, 2008; Madhumathi, Binulal, et al., 2009; Madhumathi, Shalumon, et al., 2009; Peter et al., 2010). However, HAP/cellulose composite materials have seldom been reported (Jia, Li, Ma, Sun, & Zhu, 2010; Ma et al., 2010; Wan et al., 2007).

In this work, nHAP was prepared via a simple chemical precipitation method according to report by Padilla, Izquierdo-Barba, and Vallet-Regí (2008). The resulting HAP powder was calcified at 600 °C to obtain a strong crystalline HAP. To prevent the aggregation of nanoparticles, stirring and ultrasonification method was used to disperse the HAP particles. Furthermore, the cellulose solution prepared in 7 wt.% NaOH/12 wt.% urea aqueous solution precooled to −12 °C, could make it easier for particle dispersion. It is not hard to imagine that the nanoparticle can be encaged in cellulose inclusion complexes (ICs) due to the strong hydrogen bonds interaction (Lue & Zhang, 2010). The HAP particles dispersed evenly in the cellulose matrix to fabricate inorganic–organic hybrid films, and then their structure, mechanical properties and biocompatibility were investigated. The major goal of this work was to prepare a new biomaterial, broadening the application of cellulose in the field of biomaterials.

2. Experimental

2.1. Materials

The cellulose samples (cotton linter pulp) were supplied by Hubei Chemical Fiber Co. Ltd. (Xiangfan, China). Its weight-average molecular weight (M_w) was determined by static laser light scattering (DAWN DSP, Wyatt Technology Co., US) to be 10.9×10^4. The $Ca(NO_3)\cdot 4H_2O$ and $(NH_4)_2HPO_4$ (Sinopharm Chemical Reagent Co. Ltd), NaOH, $NH_3\cdot H_2O$ and urea (Shanghai Chemical Reagent Co. Ltd., China) were used as received. All the chemical reagents were of analytical grade and used without further purification.

2.2. Preparation of HAP/celluloses nanocomposite films

The $CaCl_2$ solution was added dropwise into $(NH_4)_2H(PO_4)_2$ solution, and $NH_3\cdot H_2O$ was used to regulate the pH. The mixture was stirred vigorously, and the stirring process continued for 2 h after $CaCl_2$ solution was added completely (Madhumathi, Shalumon, et al., 2009; Tas, 2000). The HAP precursor was aged for 12 h at 25 °C, filtered and rinsed with absolute ethanol. The obtained dry particle was ground by a pestle before calcination at 600 °C. Desired amounts of HAP were added into 7 wt.% NaOH and 12 wt.% urea aqueous solution, and then the solutions were stirred vigorously for 12 h. The resultant suspensions were treated for 0.5 h through supersonication (ultrasonic instrument KQ3200). The NaOH/urea/HAP suspensions were pre-cooled to −12 °C, then the desired amounts of cellulose sample were added immediately below 25 °C. The cellulose was completely dissolved in 5 min with stirring speed at about 1500 rpm to obtain a homogeneous solution. The resulting cellulose/HAP solutions were centrifuged to degas at 1200 rpm for 15 min, and then cast on a glass plate to provide a gel sheet with a thickness of about 0.2 mm. It was immediately coagulated with a 5 wt.% Na_2SO_4 aqueous solution for 15 min to obtain blend films. The obtained films were first washed with running water and then exhaustively with deionized water to remove the urea and NaOH. The films were then dried in air at room temperature, the HAP/cellulose hybrid films were coded as RC, RCH30-1 and RCH5-1, according to the weight ratio between cellulose and HAP to be 30:1 and 5:1. The pure regenerated cellulose film was coded as RC.

2.3. Characterization

HRTEM and power spectrum observations were carried out on an electron microscope [JEOL JEM 2010 FEF (UHR), Japan] with an accelerating voltage of 200 kV. The n-HAP sample was prepared by evaporating a drop of butyl alcohol diluted suspension on a carbon-coated copper grid, and RCH5-1 film was sliced for ultrathin section without dying. FESEM (SIRION TMP, FEI) was used at an accelerating voltage of 20 kV. The films were frozen in liquid nitrogen, immediately snapped and then freeze-dried. The surface and fracture surface (cross-section) of the films was sputtered with gold, observed and then photographed. WAXD measurements were carried out on a WAXD diffractometer (D8-Advance, Bruker, USA). The patterns with Cu K_α radiation ($\lambda = 0.15406$ nm) at 40 kV and 30 mA were recorded in the region of 2θ from 4 to 55°. The samples were ground into powder and dried in a vacuum oven at 60 °C for 48 h before testing. The crystallinity X_c (%) of the HAP was estimated according to the Lorentz–Gaussian peak separation method, and was then calculated by using the following equation (Rabek, 1980):

$$x_c = \frac{\int_0^\infty s^2 I_C(s) ds}{\int_0^\infty s^2 I(s) ds} \quad (1)$$

where s is the magnitude of the reciprocal-lattice vector and it is given by $s = (2 \sin\theta)/\lambda$ the X-ray wavelength, $I(s)$ is the intensity of coherent X-ray scattering from a specimen (both crystalline and amorphous), $I_C(s)$ is the intensity of coherent X-ray scattering from the crystalline region. FT-IR spectra were carried out with a FT-IR spectrometer (1600, Perkin–Elmer Co., MA) in the wavelength range from 4000 to 400 cm^{-1}. The samples were cut into powder and then vacuum dried for 24 h before measurement. The test specimens were prepared by the KBr disk method. Thermo-gravimetric analysis (TGA) for the films was performed on a TG instrument (Perkin–Elmer Co., USA) in an atmosphere of nitrogen at a heating rate of 10 °C/min^{-1} from 30 to 600 °C. The tensile strength (σ_b) and elongation at break (ε_b) of the films in dry state were measured on a universal tensile tester (CMT 6503, Shenzhen SANS Test machine Co. Ltd., Shenzhen, China) according to ISO527-3-1995 (E) at a speed of 2 mm/min^{-1}. Because the strength data are related to the environmental temperature and humidity, these data were measured under the same conditions.

2.4. Cell viability assay

The films were sterilized with 70% ethanol and allowed to air-dry. Subsequently, the films were put into 24-well plates, and 293T cells (8×10^4 cells per well) were seeded on the surface of the sterilized cellulose matrices, and grew in 1 mL of Dulbecco's modified Eagle's medium (DMEM, Sigma) with 10% FBS at 37 °C under 5% CO_2. Images of the cells were taken at 48 h by an inverted optical microscope (IX 70, Olympus, Japan) with magnification of 100×. Cytotoxicity of 293T cells incubated on different surfaces in 24-well plates was assayed by MTT after 48 h incubation. 125 μL MTT solution (5 mg mL^{-1} in PBS) was added to each well reaching a final concentration of 1 mg mL^{-1} of MTT. The mixture was incubated for another 4 h, and then, the medium was replaced by 500 μL of dimethyl sulfoxide (DMSO). The solution in each well was mixed with a pipette, and then adopted 100 μL solution of each well for measurement. The absorbance of the solution was measured with microplate reader (BIO-RAD, Model 550, USA) at 570 nm to determine the OD value. The percent relative viability in reference to

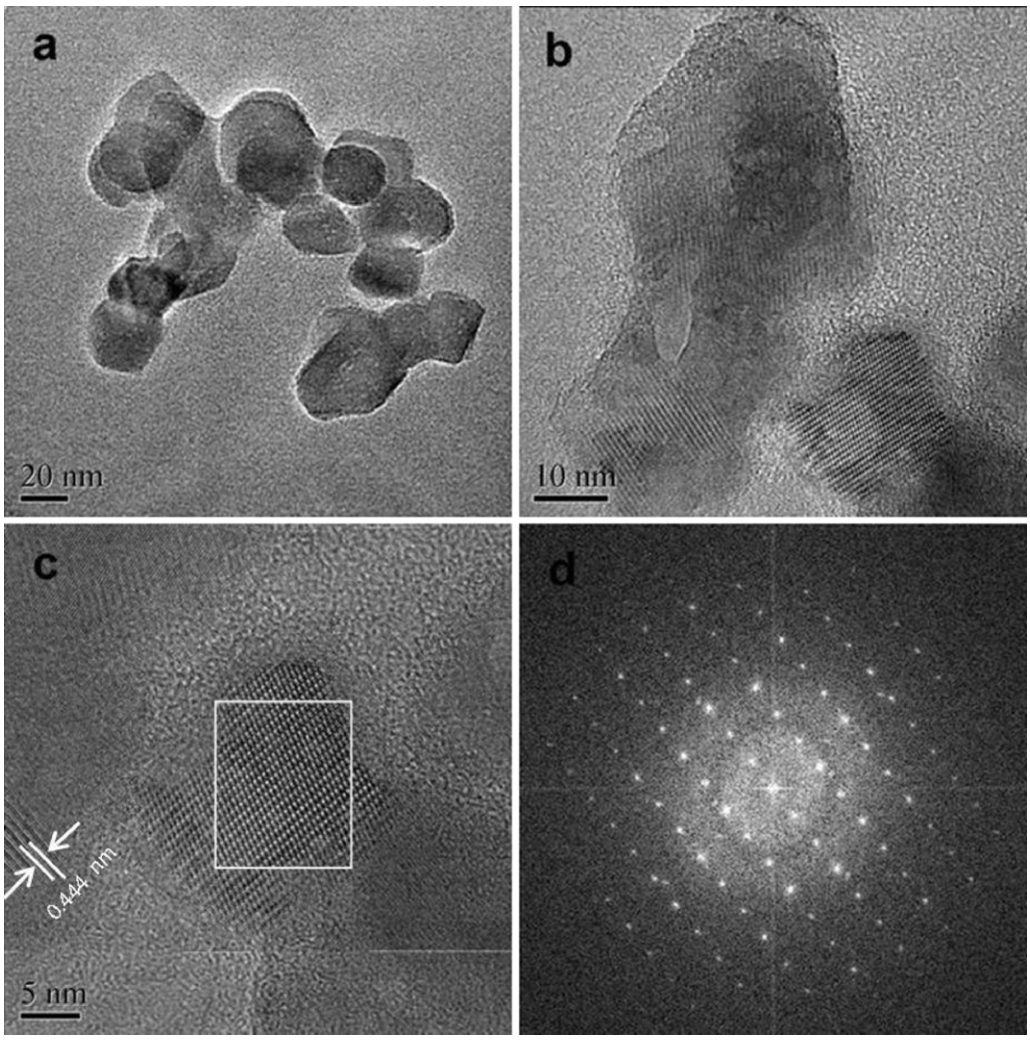

Fig. 1. HRTEM images of the HAP nanoparticles precipitated at 25 °C (a–c) and power spectrum of HAP (d).

control wells containing complete DMEM without films was calculated as follows:

$$\text{Relative cell viability}(\%) = \frac{A_{\text{test}} - A_0}{A_{\text{control}} - A_0} \times 100\% \quad (2)$$

where A is absorbance at 570 nm, A_{control} is the absorbance of the solution containing cells without films, A_0 is the absorbance of the solution containing cells and complete DMEM without MTT and film.

3. Results and discussion

3.1. Morphology and structure of hydroxyapaptite particles

Fig. 1 shows HRTEM images and power spectrum of the HAP nanoparticles. The HRTEM results indicated that the HAP nanoparticles have been successfully synthesized, and the particle size was in the range of 20–40 nm. However, the HAP nanoparticles could aggregate as the concentration was relatively high. The nHAP exhibited well crystallinity, and almost all the area was crystallized (Fig. 1b). The crystal planes and crystal zone were clearly, the lattice fringes marked representatively was about 0.444 nm (Fig. 1c, an enlargement of b). And power spectrum (of marked zone in c) displayed (1 0 1) oriented HAP, indicating that the hexagonal crystal of HAP formed rather than monoclinic (Ma & Liu, 2009; Nassif et al., 2010).

Fig. 2 shows WAXD spectra of the RC, RCH30-1, RCH5-1 films and HAP. The WAXD patterns (Fig. 2d) further indicated the crystallinity type of HAP particles, and their degree of crystallinity was about 88%. The HAP curve exhibited all of the special peaks of HAP. The peaks at 25.9, 31.8, 32.2, 34.1, 40.0 and 46.7° were assigned to (0 0 2), (2 1 1), (1 1 2), (2 0 2), (3 1 0) and (2 2 2) HAP (h k l) indices respectively, which perfectly matched the JCPDS pattern 9-432 for HAP, indicating pure HAP (Nassif et al., 2010).

3.2. Structure and miscibility of HAP/cellulose films

Fig. 3 shows photographs of RCH5-1 film under visible light and 365 nm ultraviolet light. The RC film is transparent (Liu et al., 2008), whereas RCH was white. It is noted that RCH5-1 displayed flexibility, which was resulted from the HAP nanoparticles. Interestingly, The HAP/cellulose hybrid films exhibited a strong blue emission (Zhang et al., 2009), and there were several light spots on the hybrid film under 365 nm ultraviolet light (Fig. 3b). The $CO_2^{\bullet-}$ radical impurities in the crystal might be responsible for blue emission and the light spots may be produced by the light absorption of HAP nanoparticles with small size. Fig. 4 shows the TEM image of the RCH5-1 ultrathin section. The cellulose matrix was

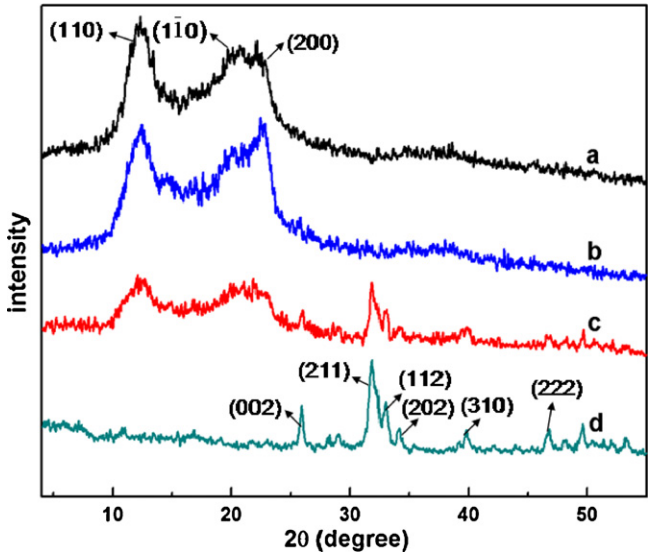

Fig. 2. WAXD spectra of the RC (a), RCH30-1 (b), RCH5-1 (c) films and HAP (d).

transparent without dying, and the HAP nanoparticles were uniformly dispersed in the hybrid film. There are homogeneous micro-and nanopores in the RC, which is a very important for the consideration of immobilizing inorganic nanoparticles and restricting the further growth of particles (Zeng, Liu, Cai, & Zhang, 2011). In our findings, the porous cellulose substrate provided pores, in which the HAP nanoparticles were fitted and immobilized, leading to the good dispersion of HAP in the inorganic–organic hybrid films. SEM images of surfaces and cross-sections of the films are shown in Fig. 5. The surface structure of cellulose films was homogeneous for RC and RCH30-1, indicating certain miscibility (Fig. 5a,b). However, with the incorporation of HAP, some particles appeared on the surface for RCH5-1, where the particles distributed evenly on the surface (Fig. 5c). There were homogeneous micro- and nanopores in the RC film, which is a very important for the consideration of immobilizing HAP particles and restricting the further growth of particles. The HAP particles emerged on RCH5-1 film surface (f), because the excess HAP particles could grow freely, resulting in the appearance of some particles (Tas, 2000).

As for 'a' in Fig. 2, three obvious crystal peaks at $2\theta = 12.2^\circ$, 19.9°, 21.1° are assigned to crystal planes (1 1 0), (1$\bar{1}$0), and (2 0 0) of cellulose II respectively (Isogai, Usuda, Kato, Uryu, & Atalla, 1989).

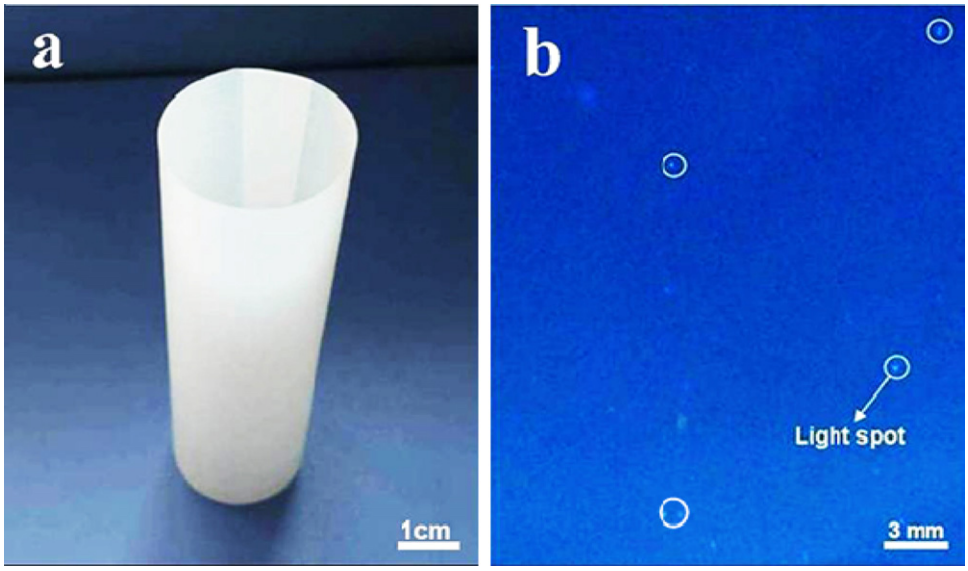

Fig. 3. Photographs of RCH5-1 film under visible light (a), and 365 nm ultraviolet light (b).

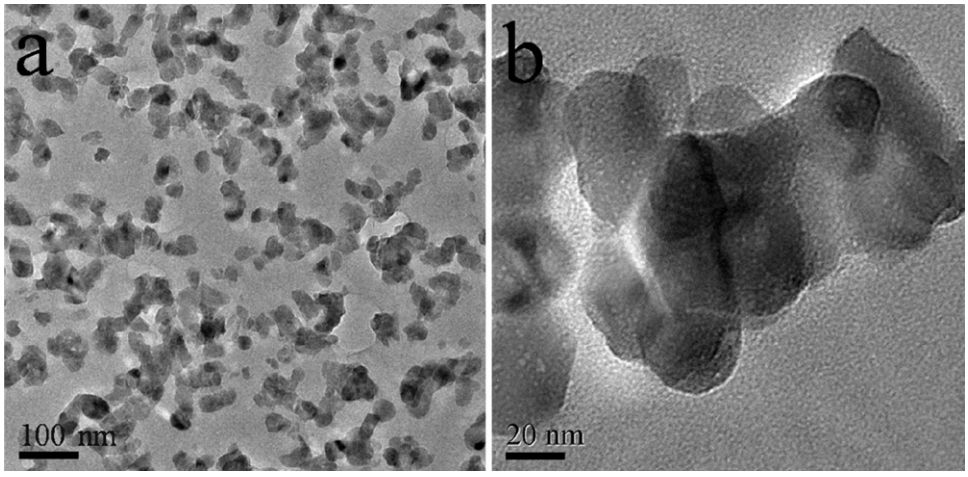

Fig. 4. HRTEM images of the RCH-5 ultrathin section (a), and the section at higher magnification (b).

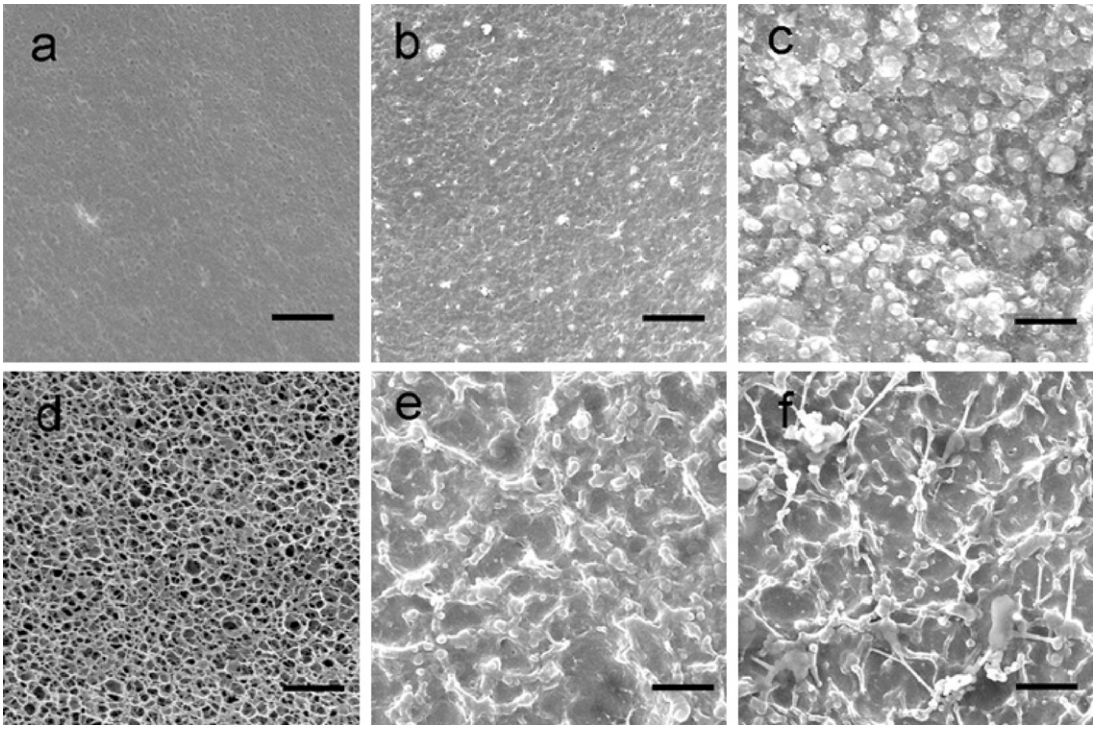

Fig. 5. FESEM images of (a–c) surface and (d–f) cross-section for RC (a,d), RCH30-1 (b,e) and RCH5-1 (c,f) films. Scale bar: 5 μm.

The curve b for RCH5-1 had obvious special peaks of the HAP and cellulose, confirming the existence of the HAP particles with native structure in the hybrid cellulose films. Interestingly, with the decrease of HAP, as shown in curve c, the peaks of HAP almost disappeared. The interaction between inorganic and organic substances has been studied using FTIR analysis. Fig. 6 shows FTIR spectra of the RC, RCH30-1, RCH5-1 films and HAP. Absorption bands for HAP (d) attributed (a) to the PO_4^{3-} group at 475 (O–P–O bending ν_2), (b) to the PO_4^{3-} group at 570 (O–P–O antisymmetric bending ν_4), 600 (O–P–O bending ν_4), 966 (P–O bending ν_1) and (c) to the adsorbed water by the broad vibrational band at 3280–3550 cm^{-1}. The shoulder at 890 cm^{-1} indicated HPO_4^{2-} incorporation into the films. The peaks of the RC and RCH films at 3300–3450 cm^{-1} corresponding to stretching vibrations of hydroxyl groups of cellulose, and the bands for RCH30-1 and RCH5-1 films broadened and shifted to low wavenumbers, indicating the strong intermolecular hydrogen bonding interaction between cellulose and HAP (Liu et al., 2008).

3.3. Properties of HAP/cellulose films

The TGA and DTG curves of the films were shown in Fig. 7. Clearly, the thermal stability of the hybrid films increased with the loading of HAP nanoparticles. The RC film began to decompose at ca. 332 °C, whereas the decomposition temperature for RCH30-1 and RCH5-1 was about 340 and 347 °C, respectively, which were higher than that of RC film. The results indicated further the strong interaction existed between the cellulose and HAP,

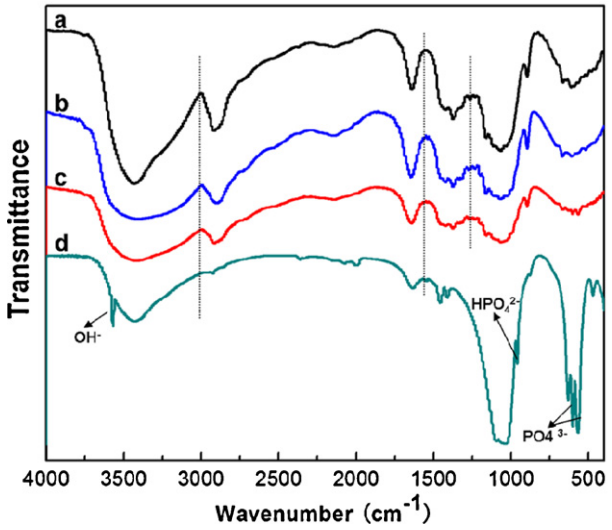

Fig. 6. FTIR spectra of the RC (a), RCH30-1 (b), RCH5-1 (c) films and HAP (d).

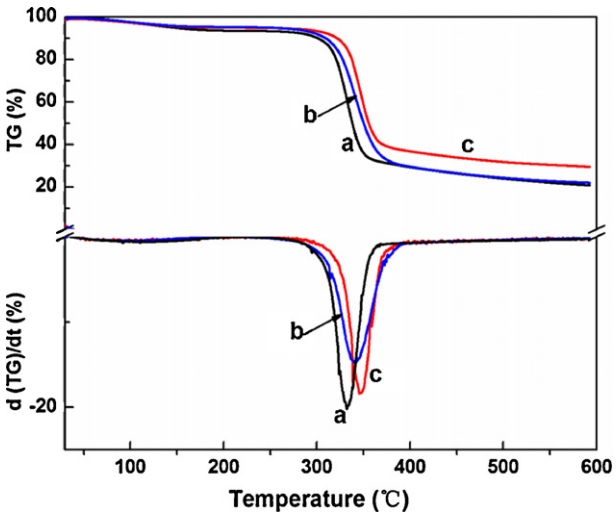

Fig. 7. TG and DTG curves of the RC (a), RCH30-1 (b) and RCH5-1 (c) films.

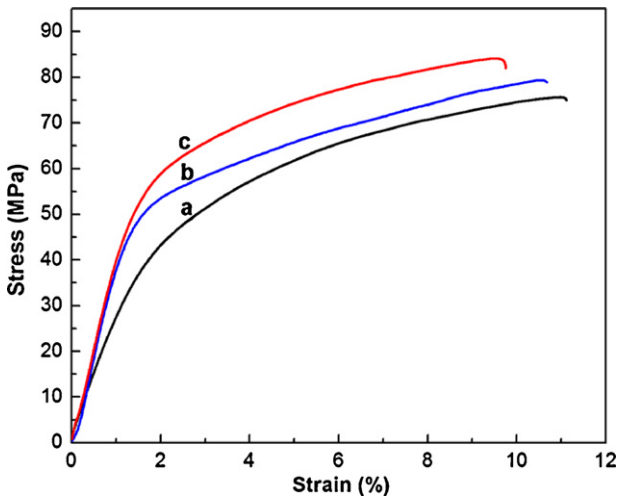

Fig. 8. Stress–strain (σ–ε) curves of the RC (a), RCH30-1 (b) and RCH5-1 (c) films.

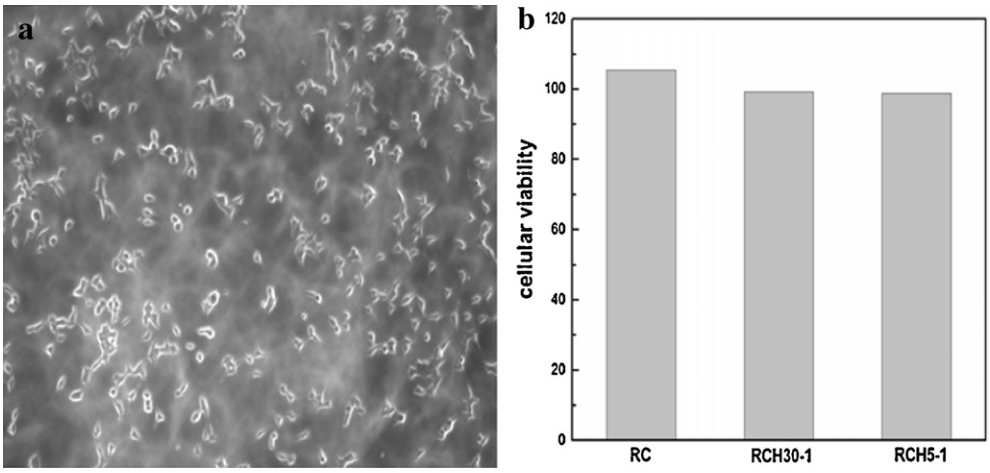

Fig. 9. Proliferation of 293T cells on the surface of the RCH30-1 hybrid film (a), and the results of the cytotoxicity tests of RC and RCH films (b).

leading to enhancement of the thermostability of the hybrid films. The mechanical properties of the films in the dry state are shown in Fig. 8. The tensile strength (σ_b) of the hybrid films increased with an increase of the HAP content, but the elongations at break (ε_b) of the hybrid films decreased slightly, compared with the RC film. The result revealed that the incorporation of HAP into the films could improve their mechanical properties, as a result of particle reinforcing effect. Moreover, the results strongly supported the conclusion on the better miscibility between cellulose and HAP from FTIR and DTG.

3.4. Biocompatibility of RCH films

The cytotoxicity of the films was evaluated in 293T cells by MTT assay. Fig. 9 shows the morphology of 293T cells on the surface of RCH30-1 composite film after 48 h incubation (a). Generally, cell adhesion to the surface of a material can be induced through the adsorbed extracellular proteins when the material is exposed to the biological fluid (Kim et al., 2007). From the images of the cells, it was found that cells spread and proliferated well on the RCH hybrid films. Good biocompatibility is necessary for the applications of the films in tissue engineering materials. Fig. 9b shows the results of the cytotoxicity of the films of RC, RCH30-1 and RCH5-1 by MTT assay. The 293T cells are quick-proliferated and adhere loosely, so the porous matrix is important for the cell adhesion and proliferation. The size of pores in RC was larger than that in RCH, so the porous RC is better for 293T cell adhesion and proliferation than MTT solution with or without RCH, and the cell viability value exceeds 100% according to Eq. (2). Obviously, the cell viability values on all films were greater than 95%, indicating excellent biocompatibility of the films to the 293T cells. This could be explained that cellulose is nontoxic, existing extensively in plants and some kinds of bacteria. Furthermore, HAP is biocompatible and bioactive and the combination of HAP and cellulose can provide enhanced bioactivity (Mathieu, Bourban, & Manson, 2006). Therefore, the HAP/cellulose hybrid films exhibited excellent proliferation of 293T cells as a result of the native macromolecules and bioactive material. The hybrid film with excellent biocompatibility, high strength and flexible properties can be utilized as a promising biomaterial.

4. Conclusion

Hydroxyapatite was successfully incorporated into the cellulose matrix in NaOH/urea aqueous system via a simple and low-cost method. The porous structure of RC film at wet state played an important role in the stabilization and dispersion of nHAP nanoparticle (20–40 nm) as a result of the strong intermolecular hydrogen bonding interaction between cellulose and HAP. The HAP nanoparticles were uniformly dispersed and immobilized in the inorganic–organic hybrid films. The HAP particles had good crystallinity and exhibited hexagonal crystal. The tensile strength and thermal stability of the HAP/cellulose hybrid films were improved significantly. In particular, the results from 293T cell culture revealed that hybrid films had non-toxicity and excellent biocompatibility, showing potential application in biomaterials.

Acknowledgements

This work was supported by National Basic Research Program of China (973 Program, 2010CB732203) and the National Natural Science Foundation of China (20874079).

References

Balasundaram, G., & Webster, T. J. (2007). An overview of nano-polymers for orthopedic applications. *Macromolecular Bioscience*, *7*(5), 635–642.

Bhardwaj, R., Mohanty, A. K., Drzal, L., Pourboghrat, F., & Misra, M. (2006). Renewable resource-based green composites from recycled cellulose fiber and poly(3-hydroxybutyrate-co-3-hydroxyvalerate) bioplastic. *Biomacromolecules*, *7*(6), 2044–2051.

Cai, J., & Zhang, L. (2005). Rapid dissolution of cellulose in LiOH/urea and NaOH/urea aqueous solutions. *Macromolecular Bioscience*, *5*(6), 539–548.

Cai, J., & Zhang, L. (2006). Unique gelation behavior of cellulose in NaOH/urea aqueous solution. *Biomacromolecules*, *7*(1), 183–189.

Cai, J., Zhang, L., Liu, S., Liu, Y., Xu, X., Chen, X., et al. (2008). Dynamic self-assembly induced rapid dissolution of cellulose at low temperatures. *Macromolecules*, *41*(23), 9345–9351.

Chang, C., Peng, J., Zhang, L., & Pang, D. W. (2009). Strongly fluorescent hydrogels with quantum dots embedded in cellulose matrices. *Journal of Materials Chemistry*, *19*(41), 7771–7776.

Cheung, H. Y., Lau, K. T., Lu, T. P., & Hui, D. (2007). A critical review on polymer-based bio-engineered materials for scaffold development. *Composites Part B: Engineering*, *38*(3), 291–300.

Colman, A., Byers, M. J., Primrose, S. B., & Lyons, A. (1978). Rapid purification of plasmid DNAs by hydroxyapatite chromatography. *European Journal of Biochemistry*, *91*(1), 303–310.

Grande, C. J., Torres, F. G., Gomez, C. M., & Carmen Bano, M. (2009). Nanocomposites of bacterial cellulose/hydroxyapatite for biomedical applications. *Acta Biomaterialia*, *5*(5), 1605–1615.

Habibi, Y., Lucia, L. A., & Rojas, O. J. (2010). Cellulose nanocrystals: Chemistry, self-assembly, and applications. *Chemical Reviews*, *110*(6), 3479–3500.

Isogai, A., Usuda, M., Kato, T., Uryu, T., & Atalla, R. H. (1989). Solid-state CP/MAS carbon-13 NMR study of cellulose polymorphs. *Macromolecules*, *22*(7), 3168–3172.

Jeong, S. I., Ko, E. K., Yum, J., Jung, C. H., Lee, Y. M., & Shin, H. (2008). Nanofibrous poly(lactic acid)/hydroxyapatite composite scaffolds for guided tissue regeneration. *Macromolecular Bioscience*, *8*(4), 328–338.

Jia, N., Li, S. M., Ma, M., Sun, R., & Zhu, J. (2010). Hydrothermal synthesis and characterization of cellulose-carbonated hydroxyapatite nanocomposites in NaOH–urea aqueous solution. *Science of Advanced Materials*, *2*(2), 210–214.

Jongpaiboonkit, L., Franklin-Ford, T., & Murphy, W. L. (2009). Growth of hydroxyapatite coatings on biodegradable polymer microspheres. *ACS Applied Materials & Interfaces*, *1*(7), 1504–1511.

Juntaro, J., Pommet, M., Kalinka, G., Mantalaris, A., Shaffer, M. S. P., & Bismarck, A. (2008). Creating hierarchical structures in renewable composites by attaching bacterial cellulose onto sisal fibers. *Advanced Materials*, *20*(16), 3122–3126.

Katti, K. S., Katti, D. R., & Dash, R. (2008). Synthesis and characterization of a novel chitosan/montmorillonite/hydroxyapatite nanocomposite for bone tissue engineering. *Biomedical Materials*, *3*, 034122.

Kim, J., Lee, K. W., Hefferan, T. E., Currier, B. L., Yaszemski, M. J., & Lu, L. (2007). Synthesis and evaluation of novel biodegradable hydrogels based on poly(ethylene glycol) and sebacic acid as tissue engineering scaffolds. *Biomacromolecules*, *9*(1), 149–157.

Liu, S., Zhang, L., Zhou, J., & Wu, R. (2008). Structure and properties of cellulose/Fe_2O_3 nanocomposite fibers spun via an effective pathway. *The Journal of Physical Chemistry C*, *112*(12), 4538–4544.

Lu, Y., & Larock, R. C. (2007). Fabrication morphology and properties of soybean oil©\based composites reinforced with continuous glass fibers. *Macromolecular Materials and Engineering*, *292*(10–11), 1085–1094.

Lue, A., & Zhang, L. (2010). Effects of carbon nanotubes on rheological behavior in cellulose solution dissolved at low temperature. *Polymer*, *51*(12), 2748–2754.

Luo, X., Liu, S., Zhou, J., & Zhang, L. (2009). In situ synthesis of Fe_3O_4/cellulose microspheres with magnetic-induced protein delivery. *Journal of Materials Chemistry*, *19*(21), 3538–3545.

Ma, G., & Liu, X. Y. (2009). Hydroxyapatite: Hexagonal or monoclinic? *Crystal Growth and Design*, *9*(7), 2991–2994.

Ma, M., Zhu, J., Jia, N., Li, S., Sun, R., Cao, S., et al. (2010). Rapid microwave-assisted synthesis and characterization of cellulose–hydroxyapatite nanocomposites in N,N-dimethylacetamide solvent. *Carbohydrate Research*, *345*(8), 1046–1050.

Madhumathi, K., Binulal, N., Nagahama, H., Tamura, H., Shalumon, K., Selvamurugan, N., et al. (2009). Preparation and characterization of novel [beta]-chitin-hydroxyapatite composite membranes for tissue engineering applications. *International Journal of Biological Macromolecules*, *44*(1), 1–5.

Madhumathi, K., Shalumon, K., Rani, V., Tamura, H., Furuike, T., Selvamurugan, N., et al. (2009). Wet chemical synthesis of chitosan hydrogel–hydroxyapatite composite membranes for tissue engineering applications. *International Journal of Biological Macromolecules*, *45*(1), 12–15.

Mathieu, L., Bourban, P. E., & Manson, J. A. E. (2006). Processing of homogeneous ceramic/polymer blends for bioresorbable composites. *Composites Science and Technology*, *66*(11–12), 1606–1614.

Murugan, R., & Ramakrishna, S. (2004). Bioresorbable composite bone paste using polysaccharide based nano hydroxyapatite. *Biomaterials*, *25*(17), 3829–3835.

Nassif, N., Martineau, F., Syzgantseva, O., Gobeaux, F., Willinger, M., Coradin, T., et al. (2010). In vivo inspired conditions to synthesize biomimetic hydroxyapatite. *Chemistry of Materials*, *22*(12), 3653–3663.

Padilla, S., Izquierdo-Barba, I., & Vallet-Regí, M. (2008). High specific surface area in nanometric carbonated hydroxyapatite. *Chemistry of Materials*, *20*(19), 5942–5944.

Peter, M., Binulal, N., Soumya, S., Nair, S., Furuike, T., Tamura, H., et al. (2010). Nanocomposite scaffolds of bioactive glass ceramic nanoparticles disseminated chitosan matrix for tissue engineering applications. *Carbohydrate Polymers*, *79*(2), 284–289.

Qi, H., Chang, C., & Zhang, L. (2008). Properties and applications of biodegradable transparent and photoluminescent cellulose films prepared via a green process. *Green Chemistry*, *11*(2), 177–184.

Rabek, J. F. (1980). *Experimental methods in polymer chemistry: Physical principles and application*. Chichester, England/New York: Wiley.

Ragauskas, A. J., Williams, C. K., Davison, B. H., Britovsek, G., Cairney, J., Eckert, C. A., et al. (2006). The path forward for biofuels and biomaterials. *Science*, *311*(5760), 484.

Ramakrishna, S., Mayer, J., Wintermantel, E., & Leong, K. W. (2001). Biomedical applications of polymer–composite materials: A review. *Composites Science and Technology*, *61*(9), 1189–1224.

Ruan, D., Zhang, L., Mao, Y., Zeng, M., & Li, X. (2004). Microporous membranes prepared from cellulose in NaOH/thiourea aqueous solution. *Journal of Membrane Science*, *241*(2), 265–274.

Schröder, E., Jönsson, J., & Poole, T. L. (2003). Hydroxyapatite chromatography: Altering the phosphate-dependent elution profile of protein as a function of pH. *Analytical Biochemistry*, *313*(1), 176–178.

Sgriccia, N., Hawley, M., & Misra, M. (2008). Characterization of natural fiber surfaces and natural fiber composites. *Composites Part A: Applied Science and Manufacturing*, *39*(10), 1632–1637.

Svagan, A. J., Samir, M. A. S., & Berglund, L. A. (2008). Biomimetic foams of high mechanical performance based on nanostructured cell walls reinforced by native cellulose nanofibrils. *Advanced Materials*, *20*(7), 1263–1269.

Swetha, M., Sahithi, K., Moorthi, A., Srinivasan, N., Ramasamy, K., & Selvamurugan, N. (2010). Biocomposites containing natural polymers and hydroxyapatite for bone tissue engineering. *International Journal of Biological Macromolecules*, *47*(1), 1–4.

Tas, C. (2000). Synthesis of biomimetic Ca-hydroxyapatite powders at 37° C in synthetic body fluids. *Biomaterials*, *21*(14), 1429–1438.

Wan, Y., Huang, Y., Yuan, C., Raman, S., Zhu, Y., Jiang, H., et al. (2007). Biomimetic synthesis of hydroxyapatite/bacterial cellulose nanocomposites for biomedical applications. *Materials Science and Engineering: C*, *27*(4), 855–864.

Wei, G., & Ma, P. X. (2004). Structure and properties of nano-hydroxyapatite/polymer composite scaffolds for bone tissue engineering. *Biomaterials*, *25*(19), 4749–4757.

Yan, L., Chen, J., & Bangal, P. R. (2007). Dissolving cellulose in a NaOH/thiourea aqueous solution: A topochemical investigation. *Macromolecular Bioscience*, *7*(9–10), 1139–1148.

Yang, Q., Lue, A., Qi, H., Sun, Y., Zhang, X., & Zhang, L. (2009). Properties and bioapplications of blended cellulose and corn protein films. *Macromolecular Bioscience*, *9*(9), 849–856.

Zeng, J., Liu, S., Cai, J., & Zhang, L. (2011). TiO_2 immobilized in cellulose matrix for photocatalytic degradation of phenol under weak UV light irradiation. *The Journal of Physical Chemistry C*, *114*(17), 7806–7811.

Zhang, C., Yang, J., Quan, Z., Yang, P., Li, C., Hou, Z., et al. (2009). Hydroxyapatite nano-and microcrystals with multiform morphologies: Controllable synthesis and luminescence properties. *Crystal Growth and Design*, *9*(6), 2725–2733.